Water Science & Technology

IWA PUBLISHING

Water Science & Technology Vol 90 No 3, 824 doi: 10.2166/wst.2024.256

Progress of metal-loaded biochar-activated persulfate for degradation of emerging organic contaminants

Tianhong Zhou[a], Chao Shi[a,b,*], Yangyang Wang[b,c], Xiaoshu Wang[c], Zhenle Lei[a], Xunjie Liu[c], Jinyu Wu[c], Fengxiang Luo[c] and Lei Wang[b,c]

[a] School of Environmental and Municipal Engineering, Lanzhou Jiaotong University, Lanzhou 730070, China
[b] Eco-Environmental Science Center (Guangdong, Hong-Kong, Macau), Guangzhou 510555, China
[c] School of Materials and Environmental Engineering, Institute of Urban Ecology and Environment Technology, Shenzhen Polytechnic University, Shenzhen 518055, China
*Corresponding author. E-mail: 17308731635@163.com

CS, 0009-0008-1919-629X

ABSTRACT

In recent years, studies on the degradation of emerging organic contaminants by sulfate radical ($SO_4^{\cdot-}$) based advanced oxidation processes (SR-AOPs) have triggered increasing attention. Metal-loaded biochar (Me-BC) can effectively prevent the agglomeration and leaching of transition metals, and its good physicochemical properties and abundant active sites induce outstanding in activating persulfate (PS) for pollutant degradation, which is of great significance in the field of advanced oxidation. In this paper, we reviewed the preparation method and stability of Me-BC, the effect of metal loading on the physicochemical properties of biochar, the pathways of pollutant degradation by Me-BC-activated PS (including free radical pathways: $SO_4^{\cdot-}$, hydroxyl radical (·OH), superoxide radicals ($O_2^{\cdot-}$); non-free radical pathways: singlet oxygen ($^1O_2$), direct electron transfer), and discussed the activation of different active sites (including metal ions, persistent free radicals, oxygen-containing functional groups, defective structures, etc.) in the SR-AOPs system. Finally, the prospect was presented for the current research progress of Me-BC in SR-AOPs technology.

Key words: active sites, advanced oxidation process, emerging organic contaminants, metal-loaded biochar, persulfate

HIGHLIGHTS

- The characteristics of the preparation methods for metal-loaded biochar are summarized.
- The effects of metals on the physicochemical properties of biochar are discussed.
- The free radical and non-radical pathways for activation of persulfate by metal-loaded biochar are discussed.
- The potential mechanisms of metal-loaded biochar catalysts are discussed.
- The future blueprint for metal-loaded is described.

1. INTRODUCTION

With the development of industrial production levels, the detection frequency of emerging organic contaminants (EOCs), such as persistent organic pollutants, endocrine disruptors, antibiotics, and microplastics, in the aquatic environment has been gradually increasing. EOCs are usually characterized by high toxicity, persistence, bioaccumulation, and long-distance transport, which pose potential hazards to the ecological environment and human health (Zhong *et al.* 2022). Sulfate radical ($SO_4^{\cdot-}$) based advanced oxidation process (SR-AOP) is a highly efficient treatment technology that shows better degradation effect in the *in situ* oxidation of EOCs and has the advantages of low cost, easy transportation, and storage, so it has been attracting great attention in the field of water treatment (Lee *et al.* 2020). SR-AOPs can fracture the O–O of persulfate (PS) to produce a reactive oxidized species $SO_4^{\cdot-}$ with strong oxidizing ability (Li *et al.* 2021). In advanced oxidation processes based on electron transfer activation, Fenton and Fenton-like systems have been hotly researched, but they have gradually shown their shortcomings. At this point, the advantages of SR-AOPs come to the fore: more transition metal species are available for PS activation than for H_2O_2 activation (Zhu *et al.* 2019), solid persulfates are safer than liquid H_2O_2 for transport and

storage (Lu *et al.* 2023), and, most importantly, $SO_4^{\cdot-}$ has a higher oxidation potential than hydroxyl radical ·OH ($SO_4^{\cdot-}$, E_0 ($SO_4^{\cdot-}/SO_4^{2-}$) = 2.60–3.10 V_{NHE}; ·OH, E_0 (·OH/OH^-) = 1.90–2.70 V_{NHE}) and longer half-life ($SO_4^{\cdot-}$: 30–40 μs; ·OH: 10^{-3} μs) (Olmez-Hanci & Arslan-Alaton 2013; Yang *et al.* 2019a), which rapidly decompose organic matter into small, low-toxicity molecular compounds up to mineralization into carbon dioxide and water.

PS, including peroxymonosulfate (PMS) and peroxydisulfate (PDS), has a very low efficiency in generating active species through self-decomposition and generally needs to be activated by external energy or catalysts. Common PS activation techniques include heat, light, alkali, transition metal activation, etc. (Lei *et al.* 2023). Among them, the transition metals activation of PS has the advantages of good catalytic performance, mild reaction, and no external energy support, but there are also shortcomings such as being easy to cause secondary pollution to the environment, difficult to recycle, and unstable activation performance. In order to overcome the limitations of environmental treatment, a variety of heterogeneous structure composite catalysts have been developed. In recent years, one of the more widely used carriers in SR-AOPs at home and abroad are carbon materials, including carbon nanotubes, graphene, carbon fibers, mesoporous carbon, active carbon, and biochar (Zhuang *et al.* 2016; Guan *et al.* 2018; Rida *et al.* 2018; Yang *et al.* 2019b; Kang & Hwang 2021; Su *et al.* 2022). Among many metal-loaded carbon materials, biochar is widely used due to its wide source, easy processing, high specific surface area (SSA), abundant oxygen-containing functional groups (OFGs), excellent acid and alkali resistance, and tunable electrons (Tian *et al.* 2021; Li *et al.* 2023b), and its enrichment of active sites such as graphitization, structural defects, and N-bonding configurations, which are able to achieve PS activation, which has attracted a wide range of attention in the research on the catalysis of peroxynitrite by biochar. Biochar is usually produced by pyrolysis under anaerobic or anoxic conditions of agricultural waste, animal manure, crop kernel shells, and waste sludge as raw materials, and is a carbonaceous solid material (Pan *et al.* 2021). The application of metal-loaded biochar (Me-BC) as a catalyst in SR-AOPs cannot only avoid the leaching and agglomeration of nanometal particles, but also exert the dual activation effect of biochar and transition metals on PS, which can significantly improve the stability and activation efficiency of the catalyst, and significantly enhance the degradation of emerging pollutants by catalyst-activated PS, which offers a promising prospect for the use of Me-BC in the resourceful utilization of solid wastes and the treatment of the water environment. This provides a broad prospect for Me-BC in solid waste resource utilization and water environment treatment.

In recent years, Me-BC-activated PS has become a relatively popular research topic. Recently, Shi *et al.* reported a review on transition metal-modified biochar-activated PS, focusing on the synthesis of different types of transition metal (or metal oxide)/biochar-based catalysts and their applications in SR-AOPs, however, the paper did not pay special attention to the interactions between the metals and the biochar, especially in terms of metal doping to change the physicochemical properties of the biochar (Shi *et al.* 2022). Li *et al.* discussed sustainable biochar activation of PS for antibiotic removal, emphasizing the removal performance of biochar and modified biochar, the potential mechanisms, and the active sites involved in the reaction (Li *et al.* 2022), while there is an insufficient discussion on the activation of PS to generate oxidative pathways under the combined action of metals and biochar at different active sites. In this work, we surveyed the published literature on the activation of PS by Me-BC, especially the latest papers published from 2014 to 2023. This paper reviews three parts, first, the preparation method of Me-BC and evaluates the stability of Me-BC; second, the effect of metal loading on the physicochemical properties of biochar, which mainly discusses the promotion of metal loading on the generation of potential active sites; and third, the mechanism of pollutant degradation by Me-BC through activation of PS is discussed, mainly the free radical pathways ($SO_4^{\cdot-}$, ·OH, and superoxide radicals $O_2^{\cdot-}$) and the non-radical pathways (singlet oxygen $^1O_2$, direct electron transfer) generated by different active sites (e.g., metal ions, persistent free radicals (PFRs), OFGs, structural defects, etc.) through the activation of PS. In addition, some challenges in the application of Me-BC to SR-AOPs technology, such as practical application, depth of research, and catalyst recovery, were noted. It is expected to provide theoretical support for Me-BC in the application of SR-AOPs.

2. PREPARATION OF METAL-LOADED BIOCHAR AND STABILIZATION OF ME-BC

The sources of biochar can be categorized into three main groups: plant sources (plant residues), animal sources (animal residues and feces), and other sources (various sludges, metal-containing solid wastes (e.g., chromium leathers), and natural polymers (chitosan), etc.) (Song *et al.* 2022), and the common transition metals that are doped into the biochar are mainly Fe, Ni, Zn, Mn, Mg, Cu, Ce, and Co. In order to prepare Me-BC catalytic materials with different requirements, a variety of preparation methods have been developed, mainly including direct pyrolysis, carbonized impregnation, chemical

reduction, biomass impregnation pyrolysis, sol–gel method, and metal enrichment by plants. Based on the literature on Me-BC, the main steps of different preparation methods of Me-BC were sorted out and summarized in this paper and illustrated in Figure 1 (Yang *et al.* 2018; Luo *et al.* 2023; Guo *et al.* 2021a; Wang *et al.* 2021; Huang *et al.* 2023b). The common point of these preparation methods is that the biochar precursors need to be pyrolytically carbonized under anaerobic or anoxic conditions (usually nitrogen gas is passed through), and the difference lies in the treatment of metal-carrier binding. In addition, the features, advantages and disadvantages, and application examples of the different preparation methods for Me-BC are presented in Table 1.

The huge SSA of biochar provides favorable conditions for the uniform loading of metals. The distribution of surface metal particles in Fe- and Mn-loaded biochar was observed by energy dispersive spectrometer (EDS) elemental energy spectroscopy (Figure 2(a) and 2(b)), and Fe@PB9 and Mn@PB9 showed small bright spots with dense and homogeneous distribution, indicating that the metal particles were evenly distributed throughout the charcoal matrix (Wang *et al.* 2022a). Similar phenomena have been observed in Me-BC prepared by other research teams (BCNi700, ZnO/BC, $CuFe_2O_4$@BC, $CoFe_2O_4$-BC), as shown in Figure 2(c) and 2(f) (Zhao *et al.* 2020; Xu *et al.* 2022; Gu *et al.* 2023; Wang *et al.* 2023a). Biochar as a carrier can improve metal dispersion and prevent metal agglomeration, and at the same time, it can inhibit metal leaching and strengthen catalyst stability, thus improving the recycling performance of the catalyst. The stability studies of different types of Me-BC in the SR-AOPs are shown in Table 2, which indicates that Me-BC is well stabilized in the degradation system, and after the first use, the leaching of metal ions accounted for a low proportion of the catalyst, and most of them could maintain more than 80% of the mineralization rate after several times of reuse (generally 3–5 times).

3. EFFECT OF METAL LOADING ON PHYSICOCHEMICAL PROPERTIES OF BIOCHAR

It has been shown that metal loading can affect the formation of biochar during pyrolysis, such as changing the elemental composition (C, H, O, N, etc.), increasing the aromaticity, decreasing the polarity, and promoting the generation of graphite-like carbon structures (Wang *et al.* 2022a), and these changes can modulate the synergistic effect between metals and

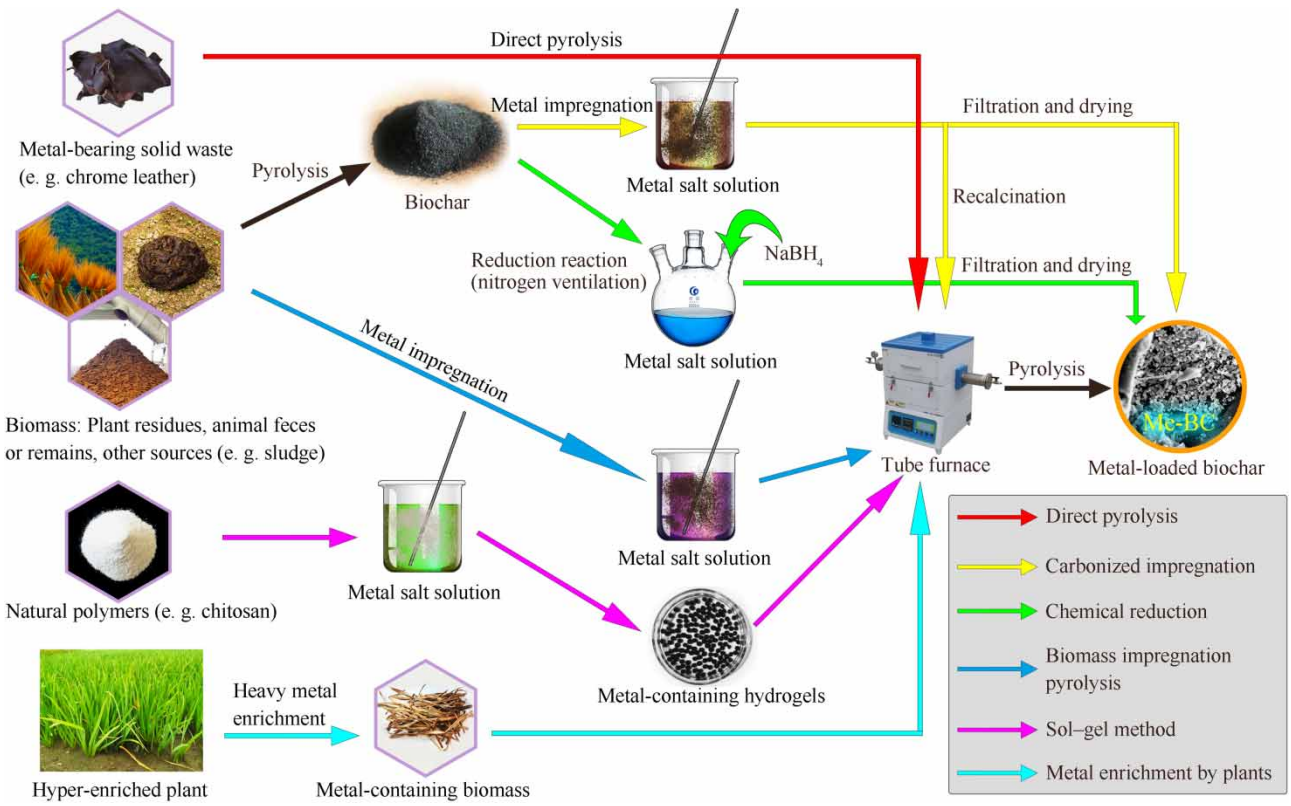

Figure 1 | The main steps of different preparation methods of Me-BC.

Table 1 | Features, advantages and disadvantages, and application examples of different preparation methods for Me-BC

Preparation method	Features	Advantages	Disadvantages	Application examples	References
Direct pyrolysis	The raw material is generally derived from metal-containing organic biomass, such as chromium-containing leather shavings	Simplest operation; conducive to solid waste resource utilization	There are few sources of raw materials that are easily restricted	Cr_2O_3/BC	Guo *et al.* (2021a)
Carbonized impregnation	A common method to prepare Me-BC by impregnating biochar into a metal salt solution	Easy to operate; loaded metal volume can be controlled	The impregnated biochar generally needs to be calcined again, which is more energy-intensive; the size and morphology of metal particles tend to be out of control	Cu_4MgO_5, nZVI-Ni@BC, BC@Fe_xC	Luo *et al.* (2023), Shan *et al.* (2021), Tong *et al.* (2022)
Chemical reduction	The reducing agent $NaBH_4$ needs to be added to the mixture of biochar and metal salt solution to enable the loaded metal to exhibit a singlet state	The loaded metal monomers have small particles, typically in the nanometer range	Requires the entire preparation process to be carried out under nitrogen gas, with high operational requirements; $NaBH_4$ is acutely toxic and chemically costly	nZVI-HCS, nZVI@Pm-BCn, BC@nZVI-Ni	Huang *et al.* (2023a), Yang *et al.* (2018), Zhu *et al.* (2020a)
Biomass impregnation pyrolysis	Common method to prepare Me-BC by impregnating biomass into a metal solution	Loaded metals improve the physicochemical properties of biochar during the pyrolysis process	The type of metal compounds loaded and their content cannot be controlled	Co-GMC, γ-Fe_2O_3@BC, biochar/Cu^0/Fe_3O_4, MMBC	Huang *et al.* (2020), Luo *et al.* (2020), Rong *et al.* (2019), Yuan *et al.* (2023)
Sol–gel method	Natural polymers such as biochar precursors, such as chitosan, are used to produce metal-containing hydrogels, which are then calcined	Biochar precursors can produce a strong chelating effect with metal ions, avoiding catalyst clumping	Complicated preparation and relatively weak catalyst stability	$CuFe_2O_4$@BC, Fe-CS@BC, Co_3O_4@BCC	Huang *et al.* (2023b), Zhao *et al.* (2020), Zhou *et al.* (2023)
Metal enrichment by plants	Me-BC precursors were obtained by using plant enrichment of metals, a method related to the study of phytoremediation in heavy metal-polluted environments	Uniform dispersion of loaded metals and stable binding to biomass; good catalyst activation performance	Uncontrollable metal loading and long preparation time	Metal@PBn, ZnO/BC, Fe⊖BC, Fe@BC	Wang *et al.* (2021, 2022a, 2022b), Xu *et al.* (2022)

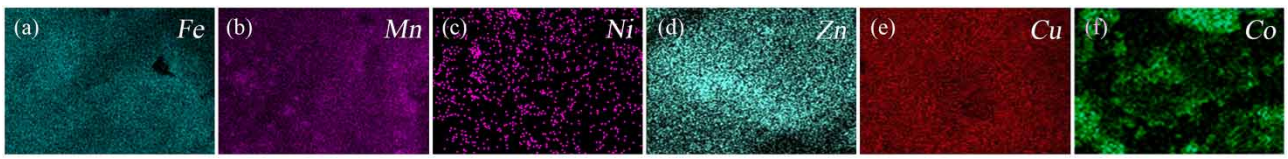

Figure 2 | Distribution of metal particles in Me-BC on the surface of biochar.

biochar and indirectly contribute to the efficiency of the pollutants degraded by the Me-BC-activated PS. The degradation rate of tetracycline (TC) by magnetite oxidized biochar OBC-Fe_3O_4 activated PS was 80.3%, which was higher than the 37.2 and 48.5% of BC/PS and OBC-Fe_3O_4/PS systems, respectively (Pi *et al.* 2019). The cobalt-loaded biochar performed excellently in

Table 2 | Stability studies of different types of Me-BC in the system of SR-AOPs

Catalyst	Degradation performance		Conditions	Leaching of metal ions after first use, % of catalyst by weight	Number of cycles, degradation rate	References
	Me-BC	BC				
CuFeBC	94.50%	5.50%	[Norfloxacin] = 30 mg/L; [PDS] = 3.0 mM; [Catalyst] = 0.5 g/L; pH = 8.5	Cu^{2+} = 2.72 mg/L, 0.54%; Fe^{3+} < 0.2 mg/L, 0.04%	4, ≥82.1%	Cai *et al.* (2023)
FeMn@N-S	92.90%	50.10%	[Tetracycline] = 40 mg/L; [PS] = 1.0 mM; [Catalyst] = 0.3 g/L; pH = 6.2	Fe^{2+}/Fe^{3+} = 0.141 mg/L, 0.047%	10, ≥80.2%	Li *et al.* (2023c)
Cu/Zn-SBC	99.28%	85.16%	[Tetracycline] = 20 mg/L; [PS] = 3.0 mM; [Catalyst] = 0.5 g/L; pH = 7.0	Cu^{2+} = 4.18 ppm, 0.836%	4, ≥77.14%	Fan *et al.* (2023)
$MnCeO_x$/TBC	98.41%	81.65%	[Tetracycline] = 10 mg/L; [PDS] = 6.0 mM; [Catalyst] = 0.8 g/L; pH = 3.0	Ce = 0.005 mg/L, 0.0006%; Mn = 0.628 mg/L, 0.079%	5, ≥94.65%	Zhang *et al.* (2022)
$MgFe_2O_4$/BC	87.87%	9.92%	[Levofloxacin] = 10 mg/L; [PDS] = 4.2 mM; [Catalyst] = 0.4 g/L; pH = 5.0	Mg = 13.2 mg/L, 3.3%; Fe = 0.38 mg/L, 0.095%	3, ≥67.90%	Yao *et al.* (2022)
nFe(0)/BC	97.68%	–	[Tetracycline] = 100 mg/L; [PDS] = 1.0 mM; [Catalyst] = 0.4 g/L; pH = 5.0	–	5, ≥86.38%	Shao *et al.* (2020)
Fe_x@biochar	100.00%	–	[2,4-Dinitrotoluene] = 14.0 μm; [PDS] = 2.5 mM; [Catalyst] = 0.5 g/L; pH = 4.05	–	5, ≥56.30%	Li *et al.* (2023a)
Ni/BC	100.00%	20.00%	[Bisphenol A] = 20 mg/L; [PDS] = 1.0 g/L; [Catalyst] = 1.5 g/L	Ni = 3.623 mg/L, 0.0024%	4, ≥88.39%	Yang *et al.* (2022)
nZVI-Ni@BC	90.70%	24.50%	[Trichloroethylene] = 0.15 mM; [PDS] = 4.0 mM; [Catalyst] = 0.25 g/L; pH = 3.4	Fe = 0.29 mg/L, 0.116%; Ni = 0.032 mg/L, 0.0128%	4, ≥85 ± 0.25%	Shan *et al.* (2021)
BM-α-FeOOH/PBC700	100.00%	16.0%	[Phenol] = 50 mg/L; [PDS] = 1.68 mM; [Catalyst] = 0.2 g/L; pH = 7.0	Fe = 0.4 mg/L, 0.2%	4, ≥82.90%	Zhao *et al.* (2022)

the degradation of antibiotics by activated PMS, and the removal of ciprofloxacin hydrochloride (CIP) by the Co-GMC/PMS system was 95.6% in 30 min, however, the GMC/PMS system without metal participation showed a lower degradation rate of 17.8% for CIP (Luo *et al.* 2020). The Fe/Mn-BC synthesized removed 83.7% of 2,4-dichlorophenol (2,4-DCP) in 30 min, which was 8.8 and 10.6 times higher than that of the pristine biochar (PBC) and Fe/Mn complexes, respectively (Zhang *et al.* 2023). Compared with the unmodified PBC, Me-BC exhibited excellent activation performance for PS, which was attributed to the activation effect of the transition metals themselves on PS on the one hand, and the modulation of the physicochemical properties of biochar by the transition metals, such as increasing the SSA and improving the pore structure, inducing the formation of metal-containing functional groups, facilitating the conversion of heteroatoms, and increasing the number of active sites, on the other hand. A specific discussion on the effect of metal loading on the physicochemical properties of biochar is presented in the following section.

3.1. Increasing specific surface area and improving pore structure

It has been reported that the degradation of pollutants may occur on the surface of biochar, and higher SSA improves the adsorption capacity of the catalyst and provides a huge area for non-homogeneous catalytic reactions, and PS adsorption that occurs on the surface of biochar is a key step in the activation (Li *et al.* 2022). Higher SSA facilitates the reduction of the electrochemical impedance of biochar, effectively promotes the electron transfer between PFRs and PS (Xu *et al.* 2022), and enhances the contribution to the non-radical pathways (Wang *et al.* 2023b). Fe-loaded biochar was prepared using plant enrichment of metals and the SSA of Fe⊙BC-4 (210.5 m^2/g) was 13 times higher than that of PBC (16.3 m^2/g)

(Wang *et al.* 2021). Others also used this method to prepare ZnO/BC at 400 °C with an SSA of 140.43 m^2/g, which was greater than that of the PBC of 82.08 m^2/g (Xu *et al.* 2022). The increase in SSA during the carbonization process was attributed to the nanoporosity created by the growth of high-density disorganized microcrystals (Oliveira *et al.* 2017), whereas the metal loading could promote the decomposition of organic compounds in biomass, and the metal dispersed into the biomass increases SSA by decreasing the degree of shrinkage of the biochar matrix, which results in the formation of a richer porous structure (Wang *et al.* 2015). Researchers pyrolyzed the metal-impregnated biomass using steam activation (CO_2) and prepared a new type of graphitic biochar composite, BC/Cu^0/Fe_3O_4 (FCBC). The results showed that the metal (oxide) entrapped in the pores could drive the carbonization of the biomass and catalyze the graphitization and decomposition of volatiles in the biochar, resulting in the formation of more pores and a more stable graphite-like structure, and the SSA, average pore diameter, and total pore volume of FCBC30 (1,240 m^2/g, 2.53 nm, and 0.79 cm^3/g) were higher than those of the PBC (1,093 m^2/g, 2.43 nm, 0.54 cm^3/g). In contrast, FCBC10 and FCBC20 containing higher metal concentrations caused pore clogging due to the overloading of Cu^0 and Fe_3O_4 metal particles, leading to a decrease in SSA, pore diameter, and total pore volume (Yuan *et al.* 2023). This suggests that moderate metal doping can increase the SSA and improve the pore structure of biochar, while excessive metal doping may lead to the opposite result.

3.2. Inducing the formation of metal-containing functional groups

Under certain conditions, some metals can form new metal-loaded stabilized structures with OFGs in biochar. Fe-loaded biochar Fe⊙BC-4 was prepared by using the plant enrichment of metals method, and XPS showed that it formed a high proportion of –C–O–Fe, which suggests the formation of a chemical bond between the biochar and Fe (Wang *et al.* 2021). The –C–O–Me bond has been reported to be essential for electron transfer via cation-π interactions (Jiang *et al.* 2018). Due to the formation of the –C–O–Fe bond, the π electrons will be transferred from the aromatic ring (electron-poor center) to the metal cation (electron-rich center), and Fe^{3+} may be reduced to Fe^{2+} by single electrons, suggesting that the –C–O–Me bond can mediate the increase in PS activation efficiency. Similarly forming –C–O–Me bonds are –C–O–Cu, –C–O–Co, Fe–O, Cu–O, etc. (Wang *et al.* 2018; Zhang *et al.* 2019; Qin *et al.* 2020; Zhao *et al.* 2020). Researchers used the biomass impregnation pyrolysis method to allow Co^{2+} to fully impregnate goat dung biomass, and a large number of hydroxyls in the lignin could chelate with the metal ions so that some of the OFGs and the metal ions tightly bound. The formation of metal-containing functional groups makes the metal firmly loaded in the biochar, which can effectively inhibit the leaching of metal ions while promoting the activation of PS (Luo *et al.* 2020).

3.3. Promoting the conversion of heteroatoms

Natural biomass generally contains non-metallic elements, such as N, P, and S, which may interact with metals to generate metal–non-metal compounds that are favorable for the activation of PS. During carbonization, a small amount of heteroatom N in biomass may interact with metals to generate metal-N bonds, such as Co–N_x, which will facilitate the deposition of Co nanoparticles and improve the stability of the catalyst (Luo *et al.* 2020). In transition metal-activated PS systems, the reduction of high-valent metals to low-valent metals is considered to be the rate-limiting step of the reaction to produce $SO_4^{\cdot-}$ and ·OH (Li *et al.* 2021), and the presence of Co–N_x as a metal-loaded stabilizing structure with a role in the reduction can promote the activation effect of Mc-BC on PS. Fe–N_x bonds are also generated in Me-BC, which are considered to be active centers with properties similar to graphite (Xu *et al.* 2021). Other non-metallic elements in natural biomass also undergo bonding reactions with metals, it was observed by XPS that cobalt-impregnated biochar contains metal-sulfur bonding compounds (Co–S), which is consistent with the results observed in X-ray diffraction (XRD) (Co_9S_8), which may show a positive effect on controlling the leaching of Co ions to, but its role in influencing the catalytic activity is still not clear (Liu *et al.* 2020a). A research team has found that their prepared Me-BC contained Fe_3S_4 and FeS (Zhu *et al.* 2022), and it is known that in the SR-AOPs, elemental S in metal sulfides serves as a provider of low valence reducing species, and S^{2-} not only accelerates the cycling of Fe(III)/Fe(II) during the activation process but also enhances the steady-state concentration of Fe(II) and controls the leaching of metal ions (Zhang *et al.* 2020; Jiang *et al.* 2023). In addition, elemental P can also form P-metal bonds with metals, and the properties of metal phosphides are similar to those of nitrides and carbides (He *et al.* 2022). Overall, the conversion of heteroatoms interacting with metals in Me-BC is beneficial for both increasing the efficiency of activating PS and further reducing the leaching of metal ions.

3.4. Regulation of the number of active sites such as PFRs, graphitization, and OFGs

The loading of metals can increase the active sites of biochar, such as PFRs, graphitization, and OFGs.

Fang *et al.* prepared catalysts using biomass impregnation pyrolysis and found that when pine needle biomass was loaded with a Fe^{3+} concentration of 0.1 mM, the concentration of PFRs within the iron-loaded biochar-activated PS system increased dramatically from 0.96×10^{19} to 4.51×10^{19} spins g^{-1}, and after adding the same concentration of other transition metals (Cu^{2+}, Ni^{2+}, and Zn^{2+}) to the biomass, the concentration of PFRs also appeared to increase to different degrees (Fang *et al.* 2015). The experimental results also demonstrated that the concentration and structure of PFRs could be regulated directionally by the appropriate addition of low concentrations of transition metals. Other research found that the cobalt-impregnated biochar CoBC contained a higher content of PFRs compared with PBC, that the electron transfer from phenolic compounds in the biomass to cobalt ions facilitated the formation of PFRs, and that the formation of PFRs was enhanced in the range of 500–800 °C. With the pyrolysis temperature rises, the PFRs in the pyrolysis products decreased sharply, indicating that the yield of PFRs was strongly affected by the pyrolysis temperature (Liu *et al.* 2020a). The experimental results of Fang *et al.* showed that the content of PFRs in Me-BC was related to the doping amount of transition metal ions and that lower concentrations of metal ions favored the formation of PFRs while excessive concentrations of metal ions depleted the PFRs, as PFRs can act as electron shuttles that mediate the reduction of transition metal ions (e.g., Fe^{3+}). The above illustrates that both the concentration of transition metal ions and the pyrolysis temperature can have a critical role in the formation of PFRs. It was found that Zn/O nanoparticles loaded in biochar could promote the secretion of PFRs precursors, such as total phenols and flavonoids organic compounds, which accelerated the formation of more oxygen-centered PFRs, which were more than the carbon-centered ones easy to activate PS, which gives it a stronger catalytic ability and longer half-life (Liu *et al.* 2020b; Xu *et al.* 2022). Fang *et al.* suggested that phenolics with one phenolic hydroxyl group or two adjacent phenolic hydroxyl groups form a stable intermediate structure with metal oxides through dehydration, and the transition metal ions accept the electrons from the phenolics for the formation of PFRs and induce an accelerated reduction of $M^{(n-1)+}$, shown in Figure 3. In addition to the generation of PFRs by the above-mentioned means, PFRs can also be formed by homolytic cleavage of chemical bonds occurring during high-temperature pyrolysis of biomass components (α- and β-alkyl-aryl ether bonds, C–C and C–O bonds) (Ouyang *et al.* 2014).

Raman spectroscopy is an important method to characterize the structural properties of carbonaceous materials. The G peak reflects the stretching motion of *sp*2 atomic pairs, which represents the ideal graphitic structure, while the D peak reflects the degree of disorder and structural defects in the crystal of the carbon atoms, and the ratio of the integrated intensities of the D and G bands (ID/IG) can be used to indicate the degree of graphitization and the integrity of the carbon material (Smith *et al.* 2016). A lower ID/IG value indicates that the carbon material has a stronger degree of graphitized structure, which is conducive to the directional flow of electrons and improves the performance of the activated PS. A variety of Me-BCs were prepared by using plant-enriched metal enrichment, at a pyrolysis temperature of 900 °C, the ID/IG values of the biochars loaded with Fe, Mn, and Zn, respectively, were significantly lower than those of the pristine biochars, which suggests that doping of the metals improved the graphitization of the biochar (Wang *et al.* 2022a). In addition, the high-resolution TEM results showed that no obvious lattice structure was found in the PBC, whereas a clear lattice structure could be observed in Me-BC, suggesting that the presence of Fe, Mn, and Zn induces the transformation of amorphous carbon into a graphite-like structure. The results of this experiment also lead to another conclusion that the ID/IG of the biochar samples decreases with increasing pyrolysis temperature, which suggests that higher pyrolysis temperatures reduce the number of structural defects and increase the degree of graphitization. The same conclusion was reached in another study (Li *et al.* 2023a),

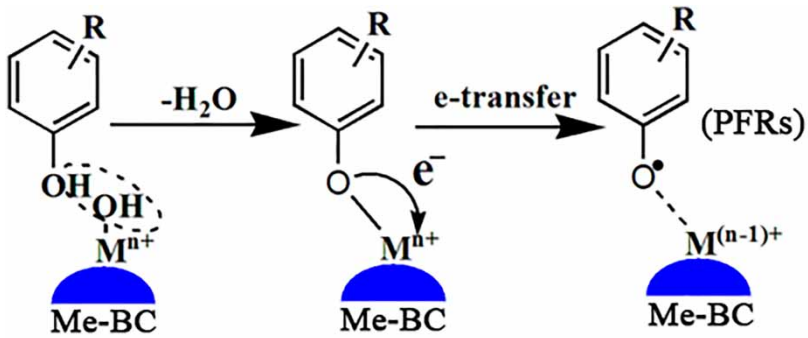

Figure 3 | Pathways of transition metal ions promoting the generation of PFRs.

where the concentration of Fe ions added to the biochar precursor was increased from 10 to 500 mM, and the ID/IG gradually decreased from 1.09 to 0.94, a result that suggests that the increase in Fe dose helps the carbon carriers to transform from defective carbon to ordered graphitic carbon. The above findings illustrate that, within a certain range, the degree of graphitization of biochar increases with the increase in pyrolysis temperature, and the loading of metal is beneficial to enhance the degree of graphitization of biochar.

Metal doping also modulates the abundance of OFGs in biochar. Comparative analysis of FeMgO/BC with PBC by XPS revealed that metal doping increased the content of C–OH and COOH in the biochar (Qin *et al.* 2020). The magnetic biochar $MgFe_2O_4$ (MMB) was characterized by FTIR spectral, and new characteristic peaks (C = C, C = O, and O = C–O) were found in MMB compared with the PBC, which indicated that the addition of $MgFe_2O_4$ significantly changed the composition of the surface OFG (Yao *et al.* 2022). A similar phenomenon has been observed in other studies, where the O–H and C–O bond strengths in Fe-loaded biochar Fex@BC increased with increasing $FeCl_3$ concentration in the biochar precursor, suggesting that Fe favors the formation of oxygen-rich functional groups (Li *et al.* 2023a). Another study found that compared with PBC the intensity of aromatic C = O peaks in Fe-loaded biochar was enhanced, which was attributed to the fact that Fe(III) promoted the formation of aromatic structures in both pyrochar and hydrochar. The results of the above-related studies suggest that the introduced metals have a significant modulating effect on OFG formation during pyrolysis (Han *et al.* 2021).

4. PATHWAYS OF POLLUTANT DEGRADATION BY ME-BC-ACTIVATED PS

The pathways of PS activation by Me-BC mainly include free radical pathways ($SO_4^{\cdot-}$, ·OH, and $O_2^{\cdot-}$) and non-radical pathways ($^1O_2$, direct electron transfer), and it is noteworthy that a large number of active sites in Me-BC play important roles in activating the PS to produce reactive oxidized species, such as redox-active transition metals, PFRs, OFGs (e.g., C = O, C–OH, –COOH, etc.), structural defects, graphitization, and N-bonded conformations. Typically, free radical pathways, $O_2^{\cdot-}$-mediated $^1O_2$ pathways, and $^1O_2$-based non-radical pathways are explored by quenching experiments coupled with electron paramagnetic resonance (EPR) analyses, whereas the electron transfer pathway is explored by electrochemical measurements. Relevant studies on Me-BC-mediated PS activation through different active sites are shown in Table 3.

4.1. Free radical pathways

The free radical pathways of $SO_4^{\cdot-}$, ·OH, and $O_2^{\cdot-}$ generation from Me-BC-activated PS mainly relied on the redox effect of transition metals, and the activation effect of active sites (PFRs, OFGs, and structural defects) in the catalyst. In this paper, by summarizing and combing the relevant literature, the pathways of free radical production from PS activation at different active sites are presented in Figure 4 (Ouyang *et al.* 2017; Liu *et al.* 2020a; Qin *et al.* 2020; Wang *et al.* 2022a).

4.1.1. Transition metals

Metal ions act as electron donors and activate PS by means of electron transfer to produce $SO_4^{\cdot-}$and ·OH, which is a free radical-based oxidation mechanism, as shown in Equations (1)–(5) (Liu *et al.* 2020a; Li *et al.* 2021). In Equations (2) and (4), the reduction of $M^{(n+1)+}$ to M^{n+} is the reaction rate-limiting step in the PS activation process, and in Equation (5) ·OH can be generated by the reaction of $SO_4^{\cdot-}$, and it was found that the main reactive oxidized species in the degradation system of Fe/Mn-BC/PDS/2,4-DCP were $SO_4^{\cdot-}$ and ·OH (Zhang *et al.* 2023), the Fe(0) content in the reacted Fe-BC decreased from 12.93 to 0%, the Fe(II) content decreased from 52.6 to 28.67%, whereas the Fe(III) content increased from 17.82 to 50.03%; the Mn(II) in the reacted Mn-BC decreased from 33.27 to 22.8%, Mn(III) from 45.42 to 34.44%, and Mn(IV) from 15.36 to 29.53% in the reacted Mn-BC. The above experimental results fully demonstrate the importance of the redox effect of metal ions in mediating the free radical pathways of PS. It has been reported that metals in the low valence state can act as electron donors to transfer electrons to dissolved oxygen in water, contributing to the generation of $O_2^{\cdot-}$ (in the case of Fe), as shown in Equation (6) (Guo *et al.* 2021b). Alternatively, $O_2^{\cdot-}$ can be generated by continued decomposition during PS activation. The hydroxylation of metal ions in Me-BC in the aqueous phase has been found to promote the generation of $SO_4^{\cdot-}$, whose preparation of Fe-loaded biochar with Fe^{2+}–BC hydroxylated in the aqueous phase to form Fe^{2+}–OH^-, forming the complex Fe^{2+}–$(HO)OSO_3^-$ by ligand substitution and finally decomposing to produce $SO_4^{\cdot-}$, as shown in

Table 3 | Relevant studies on Me-BC-mediated PS activation through different active sites

Metal	Biomass	PS	Target pollutants	Pyrolysis temperature (°C)	Active sites	Activation pathways	References
nFe_3O_4	Pine needles	PDS	1,4-Dioxane	400	Fe^{2+}/Fe^{3+}, C = C, COOH, C–OH	$SO_4^{\cdot-}$, ·OH	Ouyang *et al.* (2017)
Co^0, CoO	Goat manure	PMS	Ciprofloxacin	900	$Co^0/Co^{2+}/Co^{3+}$, graphitization, C = O	$SO_4^{\cdot-}$, ·OH, $O_2^{\cdot-}$, $^1O_2$, direct electron transfer	Luo *et al.* (2020)
γ-Fe_2O_3	Banana peel	PDS	Bisphenol A	600	Fe^{2+}/Fe^{3+}, C–OH, COOH, PFRs, structural defects, pyrrolidine N, graphitic N	$SO_4^{\cdot-}$, ·OH, $O_2^{\cdot-}$	Rong *et al.* (2019)
Fe_3O_4	*Iris sibirica* L	PDS	2,4-Dichlorophenol	500	Fe^{2+}/Fe^{3+}, C–OH, COOH, lattice oxygens	·OH, $O_2^{\cdot-}$	Wang *et al.* (2022b)
Co	Wheat straw	PMS	Atrazine	500	PFRs, Co^{2+}/Co^{3+}	$SO_4^{\cdot-}$, ·OH, $O_2^{\cdot-}$, $^1O_2$, direct electron transfer	Liu *et al.* (2020a)
MnO_x, CeO_2	Tea dregs	PDS	Tetracycline	600	Ce^{3+}/Ce^{4+}, $Mn^{2+}/Mn^{3+}/Mn^{4+}$, C–OH, C = O, lattice oxygens, structural defects	$SO_4^{\cdot-}$, ·OH, $^1O_2$, $O_2^{\cdot-}$	Zhang *et al.* (2022)
Fe^0, Fe_3O_4	Coconut shell	PDS	Arbidol	800	Fe^0, Fe_3O_4, C–OH, COOH, structural defects, graphitic N	$SO_4^{\cdot-}$, ·OH, $O_2^{\cdot-}$	Guo *et al.* (2022)
FeMgO	Cornstalks	PDS	Sulfamethazine	700	Fe^{2+}/Fe^{3+}, C–OH, COOH	$SO_4^{\cdot-}$, ·OH, $O_2^{\cdot-}$	Qin *et al.* (2020)
nZVI-Ni	Cornstalks	PDS	Trichloroethylene	500	$Fe^0/Fe^{2+}/Fe^{3+}$, Ni^+/Ni^{2+}, C–OH	$SO_4^{\cdot-}$, ·OH	Shan *et al.* (2021)
Fe	*Sedum alfredii*	PDS	Imidacloprid	900	PFRs, Fe^0/Fe^{2+}, structural defects, C = O	$SO_4^{\cdot-}$, ·OH, $^1O_2$	Wang *et al.* (2022a)

Equations (7) and (8) (Huang *et al.* 2022).

$$HSO_5^- + M^{n+} \rightarrow M^{(n+1)+} + SO_4^- \cdot + OH^- \quad (1)$$

$$HSO_5^- + M^{(n+1)+} \rightarrow M^{n+} + SO_5^- \cdot + H^+ \quad (2)$$

$$S_2O_8^{2-} + M^{n+} \rightarrow M^{(n+1)+} + SO_4^- \cdot + SO_4^{2-} \quad (3)$$

$$S_2O_8^{2-} + M^{(n+1)+} \rightarrow M^{n+} + S_2O_8^{2-} \cdot \quad (4)$$

$$SO_4^- \cdot + H_2O \rightarrow HSO_4^- + \cdot OH \quad (5)$$

$$Fe(II) + O_2 \rightarrow O_2^- \cdot + Fe(III) \quad (6)$$

$$\equiv Fe^{2+} - OH^- + HSO_5^- \longrightarrow \equiv Fe^{2+} - (HO)OSO_3^- + OH^- \quad (7)$$

$$\equiv Fe^{2+} - (HO)OSO_3^- \longrightarrow \equiv Fe^{2+} - OH^- + SO_4^- \cdot \quad (8)$$

4.1.2. Persistent free radicals

PFRs are important surface functional components of carbon-based materials (Fang *et al.* 2014a). Distinguished from transient radicals (e.g., $SO_4^{\cdot-}$ and ·OH), PFRs have a long half-life (Qin *et al.* 2018; Xie *et al.* 2024) and can also combine with transition metals (e.g., Fe, Cu, Zn, etc.) to generate stable structures. The PFRs generated during biomass pyrolysis are generally divided into two groups: oxygen-centered phenoxy and semiquinone, and carbon-centered cyclopentadienyl groups. In the Me-BC/PS system, PFRs can activate PS to produce $SO_4^{\cdot-}$ and ·OH, in addition to acting as electron donors to

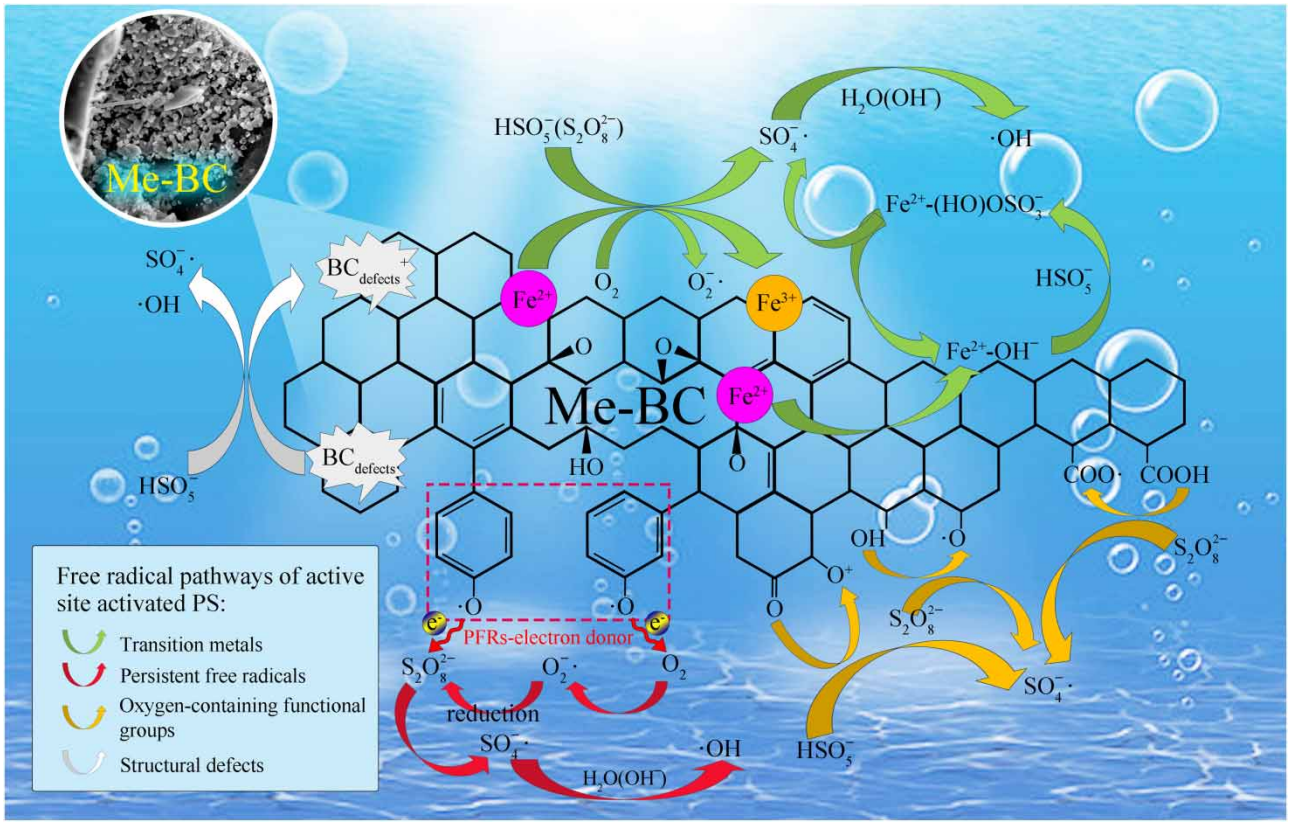

Figure 4 | Free radical pathways generated by PS activation at different active sites.

induce the transition from O_2 to $O_2^-\cdot$. Fang *et al.* used biochar impregnation pyrolysis to prepare biochars loaded with Fe, Ni, Cu, and Zn, and in the metals and biochar synergistically, the activation of PS by PFRs produced $SO_4^-\cdot$, ·OH, and ·OH, and the catalytic pathways are shown in Equations (9)–(11) (Fang *et al.* 2015): $S_2O_8^{2-}$ accepts electrons from PFRs and decomposes into $SO_4^-\cdot$; PFRs induce the transition of O_2 to $O_2^-\cdot$ through successive single electron transfers, and then $O_2^-\cdot$ reacts with $S_2O_8^{2-}$ to also produce $SO_4^-\cdot$; $SO_4^-\cdot$ reacts with H_2O or OH^- to produce ·OH. Cobalt-impregnated biochar Co/BC was prepared for the activation of PS, which suggests that PFRs can catalyze $O_2^-\cdot$ under oxygen conditions (Liu *et al.* 2020a). Other related studies have shown that the active species of the Zn200/BC/PS system are $SO_4^-\cdot$ and ·OH, and the unique single electron of PFRs is an effective site for PS activation, which accepts electrons from PFRs to form $SO_4^-\cdot$ and rapidly reacts with H_2O or OH^- to form ·OH (Xu *et al.* 2022). The above findings of both studies are in agreement with Fang *et al.*

$$BC-PFRs \xrightarrow{e^-} S_2O_8^{2-} \rightarrow SO_4^-\cdot \xrightarrow[OH^-]{H_2O} \cdot OH \quad (9)$$

$$BC-PFRs \xrightarrow{e^-} O_2 \rightarrow O_2^-\cdot \quad (10)$$

$$O_2^-\cdot + S_2O_8^{2-} \xrightarrow{\text{reduction}} SO_4^-\cdot \xrightarrow[H_2O]{OH^-} \cdot OH \quad (11)$$

4.1.3. Oxygen-containing functional group

Biochar is rich in OFGs, such as C–OH, COOH, and C = O, which can act as active sites to activate PS to produce $SO_4^-\cdot$ and ·OH. In a system of biochar-loaded nano-zero-valent iron (nFe(0)/BC) activated PS to degrade TC, it was found that $SO_4^-\cdot$ and ·OH were the dominant radicals for the degradation of TC, with the percentage of C–OH and COOH decreasing from 14.52 to 9.94% and from 25.32 to 24%, respectively, after the reaction. This result suggests that C–OH and

COOH may be involved in the activation of PS, and the activation mechanism is shown in Equations (12) and (13) (Shao *et al.* 2020). Electron-rich C = O groups can be used as electron donors, and usually, both nucleophilic C = O and electrophilic groups can activate PMS to generate reactive radicals through electron transfer between PMS and OFGs, as shown in Equation (14) (Li *et al.* 2020). In addition, C = O can also enhance the catalytic performance of PS, and electron-rich keto groups located on graphene grain boundaries are considered reactive sites, which are able to mediate redox cycling with the simultaneous generation of $SO_4^{\cdot-}$ and ·OH (electron acceptors) and $SO_5^{\cdot-}$ (electron donors) (Duan *et al.* 2017).

$$BC_{Surface} - OOH + S_2O_8^{2-} \rightarrow BC_{Surface} - OO\cdot + SO_4^{\cdot-} + HSO_4^- \quad (12)$$

$$BC_{Surface} - OH + S_2O_8^{2-} \rightarrow BC_{Surface} - O\cdot + SO_4^{\cdot-} + HSO_4^- \quad (13)$$

$$C = O + HSO_5^- \rightarrow SO_4^{\cdot-} + C - O^+ + OH^- \quad (14)$$

4.1.4. Structural defects

Structural defects are one of the active sites that activate PS to produce active species. Biochar prepared by researchers with different pyrolysis temperatures showed an increase in the degradation efficiency of 1,4-dioxane from 4.1 to 84.2% when the pyrolysis temperature was increased from 300 to 800 °C (Ouyang *et al.* 2019). It was observed by Raman spectroscopy that the ID/IG value increased from 1.79 to 2.25 with increasing pyrolysis temperature. In addition, the results of EPR combined with XPS, FTIR, and Raman analysis showed that the structural defects of the biochar (e.g., edge defects, curvature, and vacancies) create dangling σ-bonds so that its π-electrons are not restricted by the edge carbon, thus transferring electrons from the biochar to the PMS to generate $SO_4^{\cdot-}$ and ·OH. The possible mechanisms by which the structural defects activate the PMS to form free radical pathways are shown in Equations (15) and (16). The researchers concluded that high pyrolysis temperatures would eliminate excess oxygen functional groups in the biochar, which would regulate and transform the *sp*3 carbon, leading to the collapse of the carbon skeleton and the generation of more structural defects. However, other researchers came up with experimental results contrary to the above view, the ID/IG values of Fe-, Mn-, and Zn-enriched biochars, respectively, all decreased with the increase of the conditional pyrolysis temperature at 500–900 °C. The higher the pyrolysis temperature in preparation, the lower the number of structural defects and the higher the degree of graphitization (Wang *et al.* 2022a). The reason for this phenomenon may be that the doping of metals interfered with the process of pyrolytic carbonization of biomass and did not create favorable conditions for the generation of defect structures.

$$HSO_5^- + BC_{defects} \rightarrow OH^- + SO_4^{\cdot-} + BC_{defects}^+ \quad (15)$$

$$HSO_5^- + BC_{defects} \rightarrow \cdot OH + SO_4^{2-} + BC_{defects}^+ \quad (16)$$

4.2. Non-radical pathways

In the system of pollutant degradation by Me-BC-activated PS, the non-radical pathways ($^1O_2$ and direct electron transfer) oxidize the pollutants weakly compared with the free radical pathways (·OH, $SO_4^{\cdot-}$, and $O_2^{\cdot-}$), so the degradation efficiency and mineralization are lower, and it has been pointed out that the non-radical pathways mainly act in the initial stage of organic matter oxidation, and free radicals will further mineralize organic matter into CO_2 and H_2O (Xie *et al.* 2020). The non-radical pathways have higher selectivity and are less interfered with by natural organic matter and inorganic anions (NO^{3-}, HCO_3^-, halogens, etc.) (Li *et al.* 2022), which are favorable for their application in natural water and have attracted considerable attention from related scholars in recent years. In this paper, by summarizing and combing the relevant literature, the pathways of activation of PS by different active sites to generate non-radicals are presented in Figure 5 (Huggins *et al.* 2015; Huang *et al.* 2018; Liu *et al.* 2019; Yin *et al.* 2019).

4.2.1. Singlet oxygen

It has been found that $^1O_2$ can be formed by the self-decay of PS, as shown in Equation (17) (in the case of PMS) (Zhou *et al.* 2015; Wacławek *et al.* 2022). However, in the absence of catalyst acceleration, the efficiency of $^1O_2$ production via PMS self-

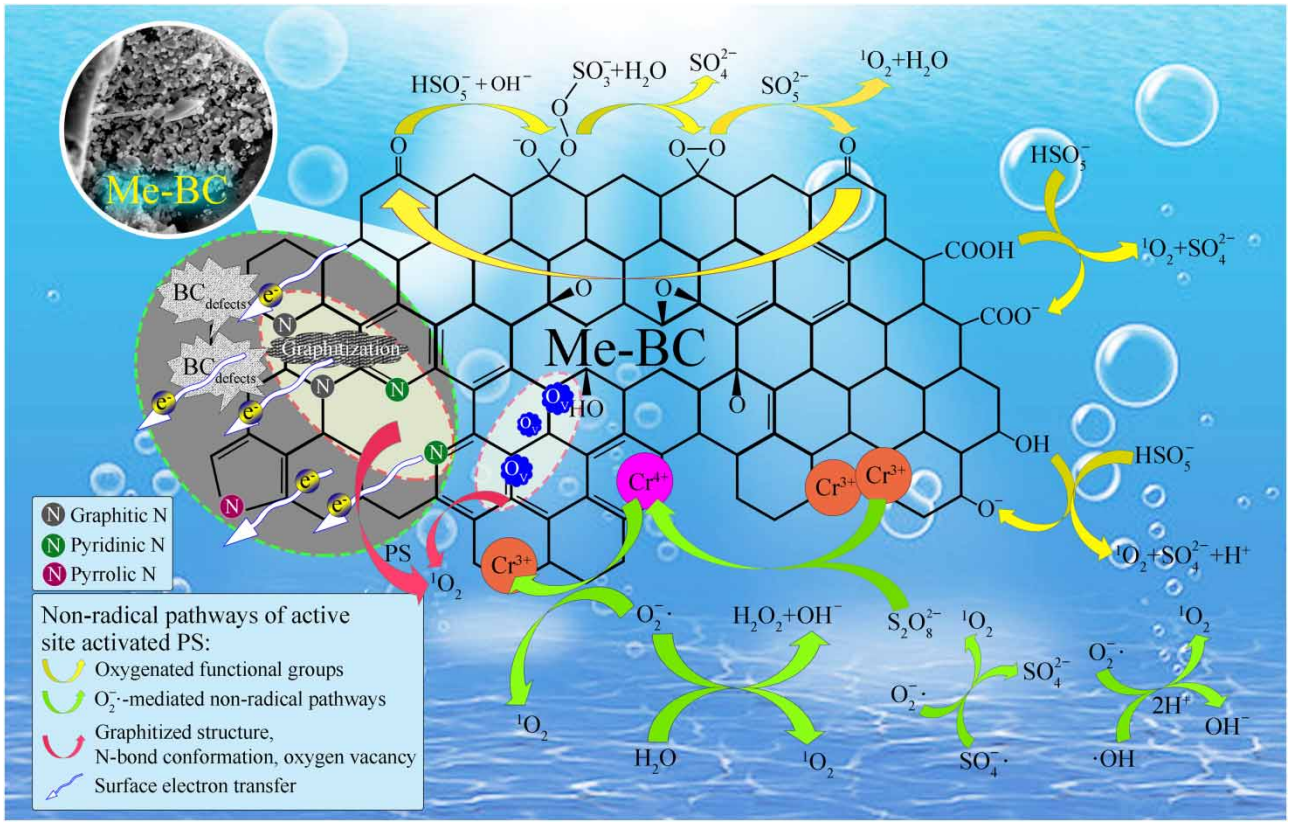

Figure 5 | Non-radical pathways generated by PS activation at different active sites.

decay is relatively low ($k = 4.7–5.9 \times 10^{-2}$ M^{-1} s^{-1}), which can hardly be the main pathway for pollution degradation by activated PS (Wacławek *et al.* 2022). Both the activation of PS by active sites and the conversion of the free radical pathways to the non-radical pathways can have a contributing effect on the production of $^1O_2$.

4.2.1.1. Activation of PS by OFGs generates singlet oxygen. Under alkaline conditions, ketone functional group-containing substances (e.g., *p*-benzoquinone, cyclohexanone) can catalyze the generation of $^1O_2$ through a cascade reaction: the nucleophilic addition reaction of PMS with ketone generates dioxane to be used as an intermediate, and the reaction of dioxane with PMS results in the recycling of ketone and the generation of $^1O_2$ (Zhou *et al.* 2015). In a related report, researchers found that metals in sludge precursors play an important role in improving the catalytic activity of biochar during sludge pyrolysis, and the results showed that the ketone group in biochar is an important active site for the generation of $^1O_2$ and that the ketone group content showed a linear relationship with the catalytic activity ($R^2 = 0.971$), and that the key steps of ketone-catalyzed PMS for the generation of $^1O_2$ were in agreement with those mentioned above, and all of them epoxy structures were formed to generate $^1O_2$ while recovering the ketone, as shown in Equations (18)–(21) (Huang *et al.* 2018). In a related study of ultra-enriched metal biochar, the C = O in the biochar adjacent to the graphite-like structure was also an important active site for the generation of $^1O_2$, and the non-radical pathways based on $^1O_2$ were activated by the breakage of the C = O double bond and its reduction under alkaline conditions, as shown in Equations (22) and (23) (Wang *et al.* 2022a). In addition to the ketone-containing functional group substances that can activate PS to produce $^1O_2$, other OFGs on the surface of biochar can also activate PMS and produce $^1O_2$. Nano-zero-valent iron biochar composites (nZVI)/biochar were excellent in activating PMS, and the removal rate of sulphamethoxazole (SMX) was as high as 100% within 20 min, which was demonstrated by the experimental results, which showed that the OFGs C–OH and COOH can mediate the non-radical pathways of PMS to produce $^1O_2$ during the conversion to C–O^- and COO^-, as shown in Equations (24) and

(25) (Huang *et al.* 2022).

$$HSO_5^- + SO_5^{2-} \rightarrow HSO_4^- + SO_4^{2-} + {}^1O_2 \quad (17)$$


(18)

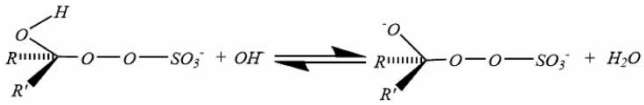
(19)

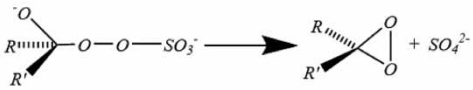
(20)

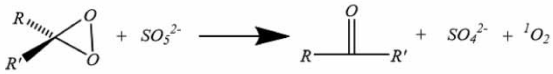
(21)

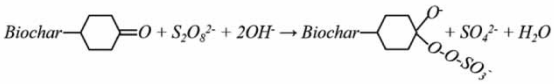
(22)

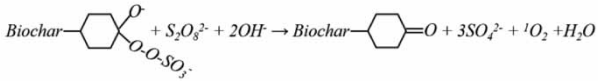
(23)

$$2BC_{surface} - OOH + 2HSO_5^- \rightarrow 2BC_{surface} - OO^- + 2SO_4^{2-} + {}^1O_2 \quad (24)$$

$$2BC_{surface} - OH + 2HSO_5^- \rightarrow 2BC_{surface} - O^- + 2SO_4^{2-} + 4H^+ + {}^1O_2 \quad (25)$$

4.2.1.2. Superoxide radical-mediated single-linear oxygen pathway. $^1O_2$ is produced by the transfer of the radical pathway to the non-radical pathway in addition to the self-decay of PS and the partial activation of OFGs. The production of $^1O_2$ involves the recombination of $O_2^-\cdot$ and the reaction with other radicals, as shown in Equations (26)–(28) (Liu *et al.* 2019; Zhu *et al.* 2020b; Wang *et al.* 2022a). Related researchers prepared magnetic rapeseed straw biochar (MRSB), which showed excellent performance in the activation of PS for TC degradation, with $^1O_2$ in the non-radical pathways playing a decisive role (Huang *et al.* 2021). Compared with the PBC, the reaction rate of the Fe_3O_4-loaded MRSB-activated PS was 13.24 times higher than that of the former, and the $^1O_2$ signals appeared in both the RSB/PS and MRSB/PS systems in the electron spin resonance (ESR) test, but the signal intensity of the latter was significantly stronger than that of the former, and these results indicated that the doping of Fe_3O_4 could enhance the composites by modulating the non-radical pathways in order to improve their catalytic activity. For Me-BC, the redox cycling of metal ions can be used as an active site to promote the formation of $^1O_2$. Other research teams prepared Cr_2O_3/BC using chromium leather chips and experimentally demonstrated that the Cr_2O_3/BC/PS system could degrade TC rapidly and efficiently, with a degradation rate as high as 99.9% within 30 min (Guo *et al.* 2021a). The high activity of Cr^{3+}/Cr^{4+} and Cr^{3+} in the carbon structure can be converted to Cr^{4+} according to the Haber–Weiss mechanism, which becomes one of the ways to accelerate the transformation of the free radical pathway ($O_2^-\cdot$) into the non-radical pathway ($^1O_2$), as shown in Equations (29) and (30), and their strong metal redox process also strengthens the free radical pathways of the activated PS.

$$2O_2^- \cdot + H_2O \rightarrow H_2O_2 + OH^- + {}^1O_2 \quad (26)$$

$$O_2^- \cdot + SO_4^- \cdot \longrightarrow {}^1O_2 + SO_4^{2-} \quad (27)$$

$$O_2^- \cdot + \cdot OH + 2H^+ \rightarrow {}^1O_2 + OH^- \quad (28)$$

$$Cr^{3+} + S_2O_8^{2-} \rightarrow Cr^{4+} + SO_4^{-} + SO_4^{2-} \quad (29)$$

$$O_2^{-}\cdot + Cr^{4+} \rightarrow {}^1O_2 + Cr^{3+} \quad (30)$$

4.2.1.3. Graphitized structures, different N-bond configurations, oxygen vacancies, and lattice oxygen promote singlet-linear oxygen production. The graphitized structure of biochar, pyridine N, graphitic N, and oxygen vacancy O_V and lattice oxygen $O_{lattice}$ in loaded metals can also serve as active sites to promote $^1O_2$ formation. It has been demonstrated that graphitized structures in carbon groups can act as active sites to activate PS to generate $^1O_2$ (Wang *et al.* 2019a; Yin *et al.* 2019), but the mechanism of how the graphitized structures mediate the generation of $^1O_2$ is not clear. In addition to the graphitized structure, different N-bond configurations can also mediate the $^1O_2$ pathway. It was found that the main active species produced by biochar NKBC800 upon activation of PS was $^1O_2$, and the reaction decreased pyridine N and graphitic N by 23.09 and 10.31%, respectively, whereas pyrrolidine N increased by 33.4%, which suggests that pyridine N and graphitic N play an important role in activating the PS-triggered non-radical pathway (Qu *et al.* 2022). Researchers prepared Fe-Ce@N-BC to activate PS (Xiao *et al.* 2022), and the relative contents of pyridine N and graphitic N in the samples decreased from 25.9 and 66.3 to 8.0 and 61.4%, respectively, after the reaction. From the degree of reduction of nitrogen species, the promotion of graphitic N in activating the PMS to generate $^1O_2$ via the non-radical pathway may be weaker than that of pyridine N, suggesting that pyridine N may be superior to graphitic N in the activation of PS. It has been reported that pyridine N has a lone pair of electrons and a high electronegativity, and carbon atoms associated with pyridine N become electron-deficient, which builds a new active catalytic site, C–N, and enhances the potential gradient, and such electron-deficient carbon atoms will react with PMS to form $^1O_2$ (Wang *et al.* 2019b). In Me-BC, O_V is also an active site that excites PS to produce $^1O_2$, and studies have shown that O_V is very active during PMS activation, and the higher density of O_V on the surface of red mud-sewage sludge derived biochar (RSDBC), as analyzed by X-ray fluorescence spectroscopy (XRF), X-ray photoelectron spectroscopy (XPS), and magnetization profile results, contributes to the $^1O_2$-dominated non-radical pathway (Wang *et al.* 2020). According to previous studies, cobalt oxide with O_V enabled $O_2^{-}\cdot$ or O_{latt}^{2-} to act as a key intermediate to facilitate the transition from O_2 to $^1O_2$ when activating PS (Li *et al.* 2021). In addition to the above, some oxygen species can also promote the formation of non-radical pathways, and abundant lattice oxygen (OI) content makes it easy to undergo a hydroxylation reaction to generate $^1O_2$. Oxygen species in catalytic materials can be classified into lattice oxygen (OI), component oxygen (OII), and oxygen in adsorbed water (OIII), and in the iron-loaded biochar Fe-RMC-850, after the reaction, the proportion of OI decreased from 51.85 to 14.11%, while the proportions of OII and OIII increased from 29.55 and 18.6 to 35.26 and 50.63%, respectively, suggesting that the catalyst undergoes a strong hydroxylation reaction in the degradation system and promotes the generation of large amounts of $^1O_2$ (Huang *et al.* 2022).

4.2.2. Direct electron transfer

Direct electron transfer occurring on the surface of Me-BC is another non-radical pathway for SR-AOPs. While adsorbing the pollutants, the biochar catalyst not only provides a huge reaction area for the degradation system but also acts as a transport medium for electron transfer, facilitating the transfer of electrons from the adsorbed pollutants (electron donors) to the PS (electron acceptors) to realize the oxidation of the pollutants.

4.2.2.1. Graphitization and defect structures promote direct electron transfer on biochar surfaces. Direct electron transfer can be reflected by the electrical conductivity (EC) of the biochar matrix, which can be promoted by some structures in biochar. It has been shown that the condensation and enlargement of aromatic rings during biochar aromatization can promote the formation of graphite-like structures with conjugated π-electron systems and that graphite-like structures can play the role of electron shuttling associated with EC (Huggins *et al.* 2015; Zhang *et al.* 2018). The related experimental result demonstrated that the activation of PDS for pollutant degradation was much more efficient with Fe/Mn-BC (83.7%) than with Fe/Mn (16%), the corrosion current density of the former ($i_{corr} = 1.72\ \mu A/cm^2$) was much higher than that of the latter ($0.218\ \mu A/cm^2$), and the graphitized structure presented in Fe/Mn-BC acted as a mediator for electron transfer to promote the activation of PDS (Zhang *et al.* 2023). It was shown that the Fe-RMC-850/PMS system was significantly higher than that of Fe-RMC-850 only (Huang *et al.* 2022), which indicated that electron transfer occurred between the

graphitized structures of Fe-RMC-850 and PMS, and the current intensity of the Fe-RMC-850/PMS/SMX system was further enhanced, suggesting that the current of Fe-RMC-850 was caused by the electron transfer between PMS and SMX. In addition to the graphitized structure that promotes surface electron transfer, it has also been reported that structural defects also induce direct electron transfer. The structural defects participate in the non-radical oxidation pathway by binding to PDS molecules to form a migratory surface-contained reactant (BC-PDS*) and the catalytic mechanism of intrinsic defect-activated PDS is the BC-PDS*-mediated electron transfer pathway (Miao *et al.* 2022). This study will provide a different interpretation of the non-radical pathways based on direct electron transfer.

4.2.2.2. Different N-bond configurations promote surface electron transfer. It has been reported that different N-bond configurations (pyridine N, pyrrolidine N, and graphitic N) can increase the Fermi energy level of carbon and enhance the electron transfer ability of carbon, thus improving the catalytic efficiency (Zhang *et al.* 2014). A number of studies have suggested that different N-bond configurations play a role in the activation of PS, but there was a lack of reliable evidence to prove exactly what activation pathways are mediated by N-bond configurations, and there is still a controversy about which N-bond type acts as what kind of active site. Rong *et al.* found that, in the system of γ-Fe_2O_3@BC/PS/BPA, the relative proportion of pyridine N after the reaction decreased from 28.5 to 26.2% and the proportion of graphitic N decreased from 50.5 to 35.3%, suggesting that pyridine N and graphitic N were involved in the reaction as active sites (Rong *et al.* 2019). Similarly, in the FeMn@N-S/PDS/TC system, XPS showed that decay peaks attributed to pyridine N and graphitic N appeared after the reaction (Li *et al.* 2023c). All these phenomena suggest that both pyridine N and graphitic N act as the main active sites in the degradation process, especially graphitic N. It has been suggested that in order to achieve electron transfer with PS, graphitic N and pyridine N can effectively increase the asymmetric spin-charge density of the nearby carbon sites, disrupting the uniform distribution of the charges and imparting positive charges to the C atoms (Duan *et al.* 2015). Iron-loaded biochar was prepared by carbonizing rabbit feces containing Fe_3O_4, and the experimental results showed that the pyridine N content decreased from 31.81% before the reaction to 15.17% after the reaction, suggesting that pyridine N was involved in the activation of PMS as the main reactive N (Huang *et al.* 2022). The results of this study showed that pyridine N was the main active N in the activation of PMS and that pyridine N was the main active N in the activation of PMS. However, there are related studies with different conclusions from the above viewpoints. It was revealed for the first time the key role of marginal nitridation in the structure of biochar: the creation of marginal nitrogen configurations (pyridine N and pyrrolidine N rather than graphitic N) led to higher EC, and faster electron transfer greatly facilitated the direct electron transfer, which provided the reaction site for the activation of PDS (Wang *et al.* 2019b).

5. CONCLUSION AND OUTLOOK

This review summarizes the research progress of Me-BC activation of PS in recent decades, with a particular focus on the important role played by different active sites in activating PS. Different Me-BC preparation methods corresponded to different requirements of the catalysts, and the combination of metal and biochar resulted in more stable catalyst performance. The metal modification of biochar adjusted the SSA, pore structure, and OFGs abundance, catalyzed active sites such as PFRs and graphitization, and broke through its catalytic limitations. The metal relies on the support of biochar, which provides a larger reaction area for its activated PS for a more uniform dispersion and may also form stable structures such as metal-containing functional groups, which reduces the agglomeration and leaching of the metal, which overcomes the drawbacks of using metal nanoparticles alone. In conclusion, Me-BC effectively modulated the interaction between metal nanoparticles and biochar to improve the stability of the catalyst as a whole, and its synergistic effect made the activated PS more efficient.

Based on the current research progress, the outlook for future research is as follows:

(1) The water treatment technology of Me-BC-activated PS should gradually tend toward practical application. Currently, most of the research work remains in laboratory batch experiments, the simulated wastewater quality is relatively single (often some difficult-to-degrade EOCs), while the actual wastewater quality is more complex, there may be a wide range of pH fluctuations, interference ions, and so on, so it is generally necessary to set up a suitable pretreatment. Whether Me-BC can be adapted to the complex environment and maintain the high efficiency of the activity remains to be further considered.

(2) It is necessary to make a toxicity assessment of the Me-BC-activated PS degradation system. On the one hand, although biochar can reduce the leaching of metal ions, the stability of some catalysts is greatly reduced under acidic conditions, contributing to increased leaching of metal ions, especially in the case of biochar loaded with heavy metals, which should be monitored as necessary. On the other hand, highly toxic intermediates may be produced during water treatment, and these toxic molecules are generally carcinogenic and mutagenic, but few researchers have analyzed the toxicity of degradation intermediates in Me-BC/PS systems, especially the antibiotic class. Therefore, in order to reduce the secondary pollution caused by the reaction, the leaching of metal ions and the toxicity of degradation intermediates in Me-BC are indispensable research topics for the future practical application of this technology.

(3) The study of active sites in SR-AOPs should be further deepened. Most of the current studies use the increase or decrease changes of active sites to judge whether they are involved in the activation process of PS, however, some studies lack sufficient evidence in the explanation of partial mechanisms, and new techniques should be developed to further analyze the roles of active sites at the molecular level in order to provide direct evidence related to free radical and non-free radical pathways.

(4) The economics of the Me-BC/PS system should be considered. The reusability and recovery of catalysts are important indicators for cost control. However, the leaching of metal ions and the loss of active sites can affect the long-term catalytic efficiency of the catalysts. Regeneration methods such as thermal regeneration and solvent regeneration have been developed to ensure reusability, but this inevitably generates a large amount of energy consumption. Therefore, Me-BC with higher stability or simple and easy-to-use regeneration methods with low energy consumption should be developed. In addition, the commonly used recovery methods are magnetic recovery and filtration recovery, however, these two recovery methods require conditions such as high magnetic properties of the catalyst itself and low impurities in the wastewater, etc., respectively, so a recovery method with high separation efficiency should be developed to improve the recovery rate of the catalyst.

ACKNOWLEDGEMENTS

This work was supported by the Shenzhen Polytechnic Project (6023310038K, 6022312023K), the Shenzhen Science and Technology Innovation Commission (KCXFZ20201221173203010, RCBS20210609104441072), and the National Natural Science Foundation of China (52200167).

AUTHOR CONTRIBUTION STATEMENT

T.Z.: Conceptualization. C.S.: Writing – original draft. Y.W.: Data curation. L.W. and X.W.: Formal analysis. X.L. and J.W.: Software. Z.L. and F.L.: Resources.

DATA AVAILABILITY STATEMENT

All relevant data are included in the paper or its Supplementary Information.

CONFLICT OF INTEREST

The authors declare there is no conflict.

REFERENCES

Cai, S., Wang, T., Wu, C., Tang, W. & Chen, J. 2023 Efficient degradation of norfloxacin using a novel biochar-supported CuO/Fe_3O_4 combined with peroxydisulfate: Insights into enhanced contribution of nonradical pathway. *Chemosphere* **329**, 138589.

Duan, X., Sun, H., Wang, Y., Kang, J. & Wang, S. 2015 N-doping-induced nonradical reaction on single-walled carbon nanotubes for catalytic phenol oxidation. *ACS Catalysis* **5** (2), 553–559.

Duan, X., Sun, H. & Wang, S. 2017 Comment on 'Activation of persulfate by graphitized nanodiamonds for removal of organic compounds'. *Environmental Science Technology* **51** (9), 5351–5352.

Fan, X., Zhang, W., Liu, Y., Shi, S., Cui, Y., Zhao, Z. & Hou, J. 2023 Hydrothermal synthesis of sewage sludge biochar for activation of persulfate for antibiotic removal: Efficiency, stability and mechanism. *Environmental Research* **218**, 114937.

Fang, G., Gao, J., Liu, C., Dionysiou, D. D., Wang, Y. & Zhou, D. 2014a Key role of persistent free radicals in hydrogen peroxide activation by biochar: Implications to organic contaminant degradation. *Environmental Science & Technology* **48** (3), 1902–1910.

Fang, Q., Chen, B., Lin, Y. & Guan, Y. 2014b Aromatic and hydrophobic surfaces of wood-derived biochar enhance perchlorate adsorption via hydrogen bonding to oxygen-containing organic groups. *Environmental Science & Technology* **48** (1), 279–288.

Fang, G., Liu, C., Gao, J., Dionysiou, D. D. & Zhou, D. 2015 Manipulation of persistent free radicals in biochar to activate persulfate for contaminant degradation. *Environmental Science & Technology* **49** (9), 5645–5653.

Gu, S., Cui, J., Liu, F. & Chen, J. 2023 Biochar loaded with cobalt ferrate activated persulfate to degrade naphthalene. *RSC Advances* **13** (8), 5283–5292.

Guan, C., Jiang, J., Luo, C., Pang, S., Yang, Y., Wang, Z., Ma, J., Yu, J. & Zhao, X. 2018 Oxidation of bromophenols by carbon nanotube activated peroxymonosulfate (PMS) and formation of brominated products: Comparison to peroxydisulfate (PDS). *Chemical Engineering Journal* **337**, 40–50.

Guo, L., Zhao, J., Zhao, L., Tang, Y., Zhou, J. & Shi, B. 2021a Persulfate activation by Cr_2O_3/BC derived from chrome shavings for antibiotics degradation. *Chemical Engineering Journal* **420**, 127698.

Guo, Y., Yan, L., Li, X., Yan, T., Song, W., Hou, T., Tong, C., Mu, J. & Xu, M. 2021b Goethite/biochar-activated peroxymonosulfate enhances tetracycline degradation: Inherent roles of radical and non-radical processes. *Science of the Total Environment* **783**, 147102.

Guo, Z., Zhang, Y., Gan, S., He, H., Cai, N., Xu, J., Guo, P., Chen, B. & Pan, X. 2022 Effective degradation of COVID-19 related drugs by biochar-supported red mud catalyst activated persulfate process: Mechanism and pathway. *Journal of Cleaner Production* **340**, 130753.

Han, L., Sun, H., Sun, K., Yang, Y., Fang, L. & Xing, B. 2021 Effect of Fe and Al ions on the production of biochar from agricultural biomass: Properties, stability and adsorption efficiency of biochar. *Renewable and Sustainable Energy Reviews* **145**, 111133.

He, Z., Zheng, W., Li, M., Liu, W., Zhang, Y. & Wang, Y. 2022 Fe_2P/biocarbon composite derived from a phosphorus-containing biomass for levofloxacin removal through peroxymonosulfate activation. *Chemical Engineering Journal* **427**, 130928.

Huang, B., Jiang, J., Huang, G. & Yu, H. 2018 Sludge biochar-based catalyst for improved pollutant degradation by activating peroxymonosulfate. *Journal of Materials Chemistry A* **6** (19), 8978–8985.

Huang, D., Zhang, Q., Zhang, C., Wang, R., Deng, R., Luo, H., Li, T., Li, J., Chen, S. & Liu, C. 2020 Mn doped magnetic biochar as persulfate activator for the degradation of tetracycline. *Chemical Engineering Journal* **391**, 123532.

Huang, H., Guo, T., Wang, K., Li, Y. & Zhang, G. 2021 Efficient activation of persulfate by a magnetic recyclable rape straw biochar catalyst for the degradation of tetracycline hydrochloride in water. *Science of the Total Environment* **758**, 143957.

Huang, W., Tang, Y., Zhang, X., Luo, Z. & Zhang, J. 2022 nZVI-biochar derived from Fe_3O_4-loaded rabbit manure for activation of peroxymonosulfate to degrade sulfamethoxazole. *Journal of Water Process Engineering* **45**, 102470.

Huang, P., Zhang, P., Wang, C., Du, X., Jia, H. & Sun, H. 2023a P-doped biochar regulates nZVI nanocracks formation for superefficient persulfate activation. *Journal of Hazardous Materials* **450**, 130999.

Huang, R., Feng, T., Wu, S., Zhang, X., Fan, Z., Yu, Q., Chen, Y. & Chen, T. 2023b In-situ synthesis of magnetic iron-chitosan-derived biochar as an efficient persulfate activator for phenol degradation. *Environmental Research* **234**, 116604.

Huggins, T. M., Pietron, J. J., Wang, H., Ren, Z. J. & Biffinger, J. C. 2015 Graphitic biochar as a cathode electrocatalyst support for microbial fuel cells. *Bioresource Technology* **195**, 147–153.

Jiang, N., Lyu, L., Yu, G., Zhang, L. & Hu, C. 2018 A dual-reaction-center Fenton-like process on -C ≡ N-Cu linkage between copper oxides and defect-containing g-C_3N_4 for efficient removal of organic pollutants. *Journal of Materials Chemistry A* **6** (36), 17819–17828.

Jiang, M., Xu, Z., Zhang, T., Zhang, X., Liu, Y., Liu, P. & Chen, X. 2023 Synergistic activation of persulfate by FeS@SBA-15 for imidacloprid degradation: Efficiencies, activation mechanism and degradation pathways. *Environmental Science and Pollution Research* **30** (30), 75595–75609.

Kang, S. & Hwang, J. 2021 $CoMn_2O_4$ embedded hollow activated carbon nanofibers as a novel peroxymonosulfate activator. *Chemical Engineering Journal* **406**, 127158.

Lee, J., Gunten, U. & Kim, J. 2020 Persulfate-based advanced oxidation: Critical assessment of opportunities and roadblocks. *Environmental Science Technology* **54** (6), 3064–3081.

Lei, Z., Song, X., Ma, G., Zhao, T., Meng, K., Zhang, M., Ren, J. & Dai, L. 2023 A review of recent studies on nano zero-valent iron activated persulfate advanced oxidation technology for the degradation of organic pollutants. *New Journal of Chemistry* **47** (31), 14585–14599.

Li, J., Li, M., Sun, H., Ao, Z., Wang, S. & Liu, S. 2020 Understanding of the oxidation behavior of benzyl alcohol by peroxymonosulfate via carbon nanotubes activation. *ACS Catalysis* **10** (6), 3516–3525.

Li, B., Wang, Y. F., Zhang, L. & Xu, H. Y. 2021 Enhancement strategies for efficient activation of persulfate by heterogeneous cobalt-containing catalysts: A review. *Chemosphere* **291**, 132954.

Li, M., Li, P., Zhou, Q. & Lee, S. L. J. 2022 A mini review on persulfate activation by sustainable biochar for the removal of antibiotics. *Materials* **15** (17), 5832.

Li, X., Cao, H., Cao, Y., Zhao, Y., Zhang, W., Shen, J., Sun, Z., Ma, F. & Gu, Q. 2023a Insights into the mechanism of persulfate activation with biochar composite loaded with Fe for 2,4-dinitrotoluene degradation. *Journal of Environmental Management* **341**, 117955.

Li, X., Zeng, J., Zuo, S., Lin, S. & Chen, G. 2023b Preparation, modification, and application of biochar in the printing field: A review. *Materials* **16** (14), 5081.

Li, Z., Chen, H., Dong, C., Jin, C., Cai, M., Chen, Y., Xie, Z., Xiong, X. & Jin, M. 2023c Nitrogen doped bimetallic sludge biochar composite for synergistic persulfate activation: Reactivity, stability and mechanisms. *Environmental Research* **229**, 115998.

Liu, S., Lai, C., Li, B., Zhang, C. & Chen, L. 2019 Role of radical and non-radical pathway in activating persulfate for degradation of *p*-nitrophenol by sulfur-doped ordered mesoporous carbon. *Chemical Engineering Journal* **384**, 123304.

Liu, B., Guo, W., Wang, H., Si, Q., Zhao, Q., Luo, H. & Ren, N. 2020a Activation of peroxymonosulfate by cobalt-impregnated biochar for atrazine degradation: The pivotal roles of persistent free radicals and ecotoxicity assessment. *Journal of Hazardous Materials* **398**, 122768.

Liu, T., Zhang, D., Yin, K., Yang, C., Luo, S. & Crittenden, J. C. 2020b Degradation of thiacloprid via unactivated peroxymonosulfate: The overlooked singlet oxygen oxidation. *Chemical Engineering Journal* **388**, 124264.

Lu, J., Lu, Q., Di, L., Zhou, Y. & Zhou, Y. 2023 Iron-based biochar as efficient persulfate activation catalyst for emerging pollutants removal: A review. *Chinese Chemical Letters* **34** (11), 108357.

Luo, J., Bo, S., Qin, Y., An, Q., Xiao, Z. & Zhai, S. 2020 Transforming goat manure into surface-loaded cobalt/biochar as PMS activator for highly efficient ciprofloxacin degradation. *Chemical Engineering Journal* **395**, 125063.

Luo, H., Wan, Y., Li, J., Cai, Y., Dang, Z. & Yin, H. 2023 Mg_xCu-biochar activated peroxydisulfate triggers reductive species for the reduction and enhanced electron-transfer degradation of electron-deficient aromatic pollutants. *Journal of Hazardous Materials* **452**, 131267.

Miao, X., Chen, X., Wu, W., Lin, D. & Yang, K. 2022 Intrinsic defects enhanced biochar/peroxydisulfate oxidation capacity through electron-transfer regime. *Chemical Engineering Journal* **438**, 135606.

Oliveira, F. R., Patel, A. K., Jaisi, D. P., Adhikari, S., Lu, H. & Khanal, S. K. 2017 Environmental application of biochar: Current status and perspectives. *Bioresource Technology* **246**, 110–122.

Olmez-Hanci, T. & Arslan-Alaton, I. 2013 Comparison of sulfate and hydroxyl radical based advanced oxidation of phenol. *Chemical Engineering Journal* **224**, 10–16.

Ouyang, D., Yan, J., Qian, L., Chen, Y., Han, L., Su, A., Zhang, W., Ni, H. & Chen, M. 2017 Degradation of 1,4-dioxane by biochar supported nano magnetite particles activating persulfate. *Chemosphere* **184**, 609–617.

Ouyang, X.-p., Tan, Y.-d. & Qiu, X.-q. 2014 Oxidative degradation of lignin for producing monophenolic compounds. *Journal of Fuel Chemistry and Technology* **42** (6), 677–682.

Ouyang, D., Chen, Y., Yan, J., Qian, L., Han, L. & Chen, M. 2019 Activation mechanism of peroxymonosulfate by biochar for catalytic degradation of 1,4-dioxane: Important role of biochar defect structures. *Chemical Engineering Journal* **370**, 614–624.

Pan, X., Gu, Z., Chen, W. & Li, Q. 2021 Preparation of biochar and biochar composites and their application in a Fenton-like process for wastewater decontamination: A review. *Science of The Total Environment* **754**, 142104.

Pi, Z., Li, X., Wang, D., Xu, Q., Tao, Z., Huang, X., Yao, F., Wu, Y., He, L. & Yang, Q. 2019 Persulfate activation by oxidation biochar supported magnetite particles for tetracycline removal: Performance and degradation pathway. *Journal of Cleaner Production* **235**, 1103–1115.

Qin, Y., Li, G., Gao, Y., Zhang, L., Ok, Y. S. & An, T. 2018 Persistent free radicals in carbon-based materials on transformation of refractory organic contaminants (ROCs) in water: A critical review. *Water Research* **137**, 130–143.

Qin, F., Peng, Y., Song, G., Fang, Q., Wang, R., Zhang, C., Zeng, G., Huang, D., Lai, C., Zhou, Y., Tan, X., Cheng, M. & Liu, S. 2020 Degradation of sulfamethazine by biochar-supported bimetallic oxide/persulfate system in natural water: Performance and reaction mechanism. *Journal of Hazardous Materials* **398**, 122816.

Qu, S., Yuan, Y., Yang, X., Xu, H., Mohamed, A. K., Zhang, J., Zhao, C., Liu, L., Wang, B. & Wang, X. 2022 Carbon defects in biochar facilitated nitrogen doping: The significant role of pyridinic nitrogen in peroxymonosulfate activation and ciprofloxacin degradation. *Chemical Engineering Journal* **441**, 135864.

Rida, T., Othmane, A., Younes, E., Karim, D., Abdallah, R. & Mohamed, Z. 2018 Magnetic $CoFe_2O_4$ nanoparticles supported on graphene oxide ($CoFe_2O_4$/GO) with high catalytic activity for peroxymonosulfate activation and degradation of rhodamine B. *RSC Advances* **8** (3), 1351–1360.

Rong, X., Xie, M., Kong, L., Natarajan, V., Ma, L. & Zhan, J. 2019 The magnetic biochar derived from banana peels as a persulfate activator for organic contaminants degradation. *Chemical Engineering Journal* **372**, 294–303.

Shan, A., Idrees, A., Zaman, W. Q., Abbas, Z., Ali, M., Rehman, M. S. U., Hussain, S., Danish, M., Gu, X. & Lyu, S. 2021 Synthesis of nZVI-Ni@BC composite as a stable catalyst to activate persulfate: Trichloroethylene degradation and insight mechanism. *Journal of Environmental Chemical Engineering* **9** (1), 104808.

Shao, F., Wang, Y., Mao, Y., Shao, T. & Shang, J. 2020 Degradation of tetracycline in water by biochar supported nanosized iron activated persulfate. *Chemosphere* **261**, 127844.

Shi, Q., Deng, S., Zheng, Y., Du, Y., Li, L., Yang, S., Zhang, G., Du, L., Wang, G., Cheng, M. & Liu, Y. 2022 The application of transition metal-modified biochar in sulfate radical based advanced oxidation processes. *Environmental Research* **212**, 113340.

Smith, M. W., Dallmeyer, I., Johnson, T. J., Brauer, C. S., McEwen, J.-S., Espinal, J. F. & Garcia-Perez, M. 2016 Structural analysis of char by Raman spectroscopy: Improving band assignments through computational calculations from first principles. *Carbon* **100**, 678–692.

Song, G., Qin, F., Yu, J., Tang, L., Pang, Y., Zhang, C., Wang, J. & Deng, L. 2022 Tailoring biochar for persulfate-based environmental catalysis: Impact of biomass feedstocks. *Journal of Hazardous Materials* **424**, 127663.

Su, X., Guo, Y., Yan, L., Wang, Q., Zhang, W., Li, X., Song, W., Li, Y. & Liu, G. 2022 MoS_2 nanosheets vertically aligned on biochar as a robust peroxymonosulfate activator for removal of tetracycline. *Separation and Purification Technology* **282**, 120118.

Tian, X., Wang, D., Chai, G., Zhang, J. & Zhao, X. 2021 Does biochar inhibit the bioavailability and bioaccumulation of As and Cd in co-contaminated soils? A meta-analysis. *Science of the Total Environment* **762**, 143117.

Tong, J., Chen, L., Cao, J., Yang, Z., Xiong, W., Jia, M., Xiang, Y. & Peng, H. 2022 Biochar supported magnetic MIL-53-Fe derivatives as an efficient catalyst for peroxydisulfate activation towards antibiotics degradation. *Separation and Purification Technology* **294**, 121064.

Wacławek, S., Lutze, H. V., Sharma, V. K., Xiao, R. & Dionysiou, D. D. 2022 Revisit the alkaline activation of peroxydisulfate and peroxymonosulfate. *Current Opinion in Chemical Engineering* **37**, 100854.

Wang, Y., Zhao, H. & Zhao, G. 2015 Iron-copper bimetallic nanoparticles embedded within ordered mesoporous carbon as effective and stable heterogeneous Fenton catalyst for the degradation of organic contaminants. *Applied Catalysis B: Environmental* **164**, 396–406.

Wang, Y., Liu, C., Zhang, Y., Meng, W., Yu, B., Pu, S., Yuan, D., Qi, F., Xu, B. & Chu, W. 2018 Sulfate radical-based photo-Fenton reaction derived by cubi$_2$o$_4$ and its composites with α-Bi_2O_3 under visible light irradiation: Catalyst fabrication, performance and reaction mechanism. *Applied Catalysis B: Environmental* **235**, 264–273.

Wang, B., Li, Y. & Wang, L. 2019a Metal-free activation of persulfates by corn stalk biochar for the degradation of antibiotic norfloxacin: Activation factors and degradation mechanism. *Chemosphere* **237**, 124454.

Wang, H., Guo, W., Liu, B., Wu, Q., Luo, H., Zhao, Q., Si, Q., Sseguya, F. & Ren, N. 2019b Edge-nitrogenated biochar for efficient peroxydisulfate activation: An electron transfer mechanism. *Water Research* **160**, 405–414.

Wang, J., Shen, M., Wang, H., Du, Y., Zhou, X., Liao, Z., Wang, H. & Chen, Z. 2020 Red mud modified sludge biochar for the activation of peroxymonosulfate: Singlet oxygen dominated mechanism and toxicity prediction. *Science of the Total Environment* **740**, 140388.

Wang, Y., Wang, L., Zhang, Y., Mao, X., Tan, W., Zhang, Y., Wang, X., Chang, M., Guo, R. & Xi, B. 2021 Perdisulfate-assisted advanced oxidation of 2,4-dichlorophenol by bio-inspired iron encapsulated biochar catalyst. *Journal of Colloid and Interface Science* **592**, 358–370.

Wang, X., Zhang, P., Wang, C., Jia, H., Shang, X., Tang, J. & Sun, H. 2022a Metal-rich hyperaccumulator-derived biochar as an efficient persulfate activator: Role of intrinsic metals (Fe, Mn and Zn) in regulating characteristics, performance and reaction mechanisms. *Journal of Hazardous Materials* **424**, 127225.

Wang, Y., Xu, J., Wang, X., Li, T., Zhang, G., Yan, Z., Liu, J. & Wang, L. 2022b Biomimetic synthesis technology for preparation of Fe_3O_4-encapsulated biochar using in highly efficient peroxodisulfate activation. *Frontiers in Chemistry* **10**, 967589.

Wang, L., Liu, X., Wang, Y. & Wang, X. 2023a Stability and ecological risk assessment of nickel (Ni) in phytoremediation-derived biochar. *Science of the Total Environment* **903**, 166498.

Wang, R., Zhang, S., Chen, H., He, Z., Cao, G., Wang, K., Li, F., Ren, N., Xing, D. & Ho, S.-H. 2023b Enhancing biochar-based nonradical persulfate activation using data-driven techniques. *Environmental Science & Technology* **57** (9), 4050–4059.

Xiao, K., Liang, F., Liang, J., Xu, W., Liu, Z., Chen, B., Jiang, X., Wu, X., Xu, J., Beiyuan, J. & Wang, H. 2022 Magnetic bimetallic Fe, Ce-embedded N-enriched porous biochar for peroxymonosulfate activation in metronidazole degradation: Applications, mechanism insight and toxicity evaluation. *Chemical Engineering Journal* **433**, 134387.

Xie, Y., Hu, W., Wang, X., Tong, W., Li, P., Zhou, H., Wang, Y. & Zhang, Y. 2020 Molten salt induced nitrogen-doped biochar nanosheets as highly efficient peroxymonosulfate catalyst for organic pollutant degradation. *Environmental Pollution* **260**, 114053.

Xie, J., Latif, J., Yang, K., Wang, Z., Zhu, L., Yang, H., Qin, J., Ni, Z., Jia, H., Xin, W. & Li, X. 2024 A state-of-art review on the redox activity of persistent free radicals in biochar. *Water Research* **255**, 121516.

Xu, H., Gao, M., Hu, X., Chen, Y., Li, Y., Xu, X., Zhang, R., Yang, X., Tang, C. & Hu, X. 2021 A novel preparation of S-nZVI and its high efficient removal of Cr(VI) in aqueous solution. *Journal of Hazardous Materials* **416**, 125924.

Xu, R., Li, M. & Zhang, Q. 2022 Collaborative optimization for the performance of ZnO/biochar composites on persulfate activation through plant enrichment-pyrolysis method. *Chemical Engineering Journal* **429**, 132294.

Yang, F., Zhang, S., Sun, Y., Cheng, K., Li, J. & Tsang, D. C. W. 2018 Fabrication and characterization of hydrophilic corn stalk biochar-supported nanoscale zero-valent iron composites for efficient metal removal. *Bioresource Technology* **265**, 490–497.

Yang, J., Liu, X., Wang, D., Xu, Q., Yang, Q., Zeng, G., Li, X., Liu, Y., Gong, J., Ye, J. & Li, H. 2019a Mechanisms of peroxymonosulfate pretreatment enhancing production of short-chain fatty acids from waste activated sludge. *Water Research* **148**, 239–249.

Yang, Z., Li, Y., Zhang, X., Cui, X. & Ding, A. 2019b Sludge activated carbon-based $CoFe_2O_4$-SAC nanocomposites used as heterogeneous catalysts for degrading antibiotic norfloxacin through activating peroxymonosulfate. *Chemical Engineering Journal* **384**, 123319.

Yang, S., Zhang, S., Xu, Q., Liu, J., Zhong, C., Xie, Z. & Zhao, Y. 2022 Efficient activation of persulfate by nickel-supported cherry core biochar composite for removal of bisphenol A. *Journal of Environmental Management* **324**, 116305.

Yao, B., Luo, Z., Du, S., Yang, J., Zhi, D. & Zhou, Y. 2022 Magnetic $MgFe_2O_4$/biochar derived from pomelo peel as a persulfate activator for levofloxacin degradation: Effects and mechanistic consideration. *Bioresource Technology* **346**, 126547.

Yin, R., Guo, W., Wang, H., Du, J., Wu, Q., Chang, J.-S. & Ren, N. 2019 Singlet oxygen-dominated peroxydisulfate activation by sludge-derived biochar for sulfamethoxazole degradation through a nonradical oxidation pathway: Performance and mechanism. *Chemical Engineering Journal* **357**, 589–599.

Yuan, Y., Zhang, C., Zhao, C., Wang, B., Wang, X., Gao, B., Wang, S. & Rinklebe, J. 2023 One-step preparation of a novel graphitic biochar/Cu^0/Fe_3O_4 composite using CO_2-ambiance pyrolysis to activate peroxydisulfate for dye degradation. *Journal of Environmental Sciences* **125**, 26–36.

Zhang, L., Su, Z., Jiang, F., Yang, L., Qian, J., Zhou, Y., Li, W. & Hong, M. 2014 Highly graphitized nitrogen-doped porous carbon nanopolyhedra derived from ZIF-8 nanocrystals as efficient electrocatalysts for oxygen reduction reactions. *Nanoscale* **6** (12), 6590–6602.

Zhang, Y., Xu, X., Cao, L., Sik, O. Y. & Xinde, C. 2018 Characterization and quantification of electron donating capacity and its structure dependence in biochar derived from three waste biomasses. *Chemosphere* **211**, 1073–1081.

Zhang, Y., Li, Q., Long, Y., Zou, J. & Chen, Z. 2019 Catalytic ozonation benefit from the enhancement of electron transfer by the coupling of g-C_3N_4 and $LaCoO_3$: Discussion on catalyst fabrication and electron transfer pathway. *Applied Catalysis B: Environmental* **254**, 569–579.

Zhang, Y., Liu, N., Yang, Y., Li, J., Wang, S., Lv, J. & Tang, R. 2020 Novel carbothermal synthesis of Fe, N co-doped oak wood biochar (Fe/N-OB) for fast and effective Cr(VI) removal. *Colloids and Surfaces A: Physicochemical and Engineering Aspects* **600**, 124926.

Zhang, Q., Song, J., Zhang, Y., Kang, X., Xu, X. & Wang, L. 2022 Preparation of $MnCeO_x$-modified tea waste biochar as peroxodisulfate activator for tetracycline degradation. *Journal of Water Process Engineering* **50**, 103209.

Zhang, K., Huang, D., Zhang, Y., El Houda Bouroubi, N., Chen, P., Ganbold, N., He, P., Liu, J., Fang, Y., Gan, M., Zhu, J. & Yang, B. 2023 Natural mineral-derived Fe/Mn-BC as efficient peroxydisulfate activator for 2,4-dichlorophenol removal from wastewater: Performance and sustainable catalytic mechanism. *Journal of Environmental Management* **335**, 117540.

Zhao, Y., Song, M., Cao, Q., Sun, P., Chen, Y. & Meng, F. 2020 The superoxide radicals' production via persulfate activated with $CuFe_2O_4$@Biochar composites to promote the redox pairs cycling for efficient degradation of *o*-nitrochlorobenzene in soil. *Journal of Hazardous Materials* **400**, 122887.

Zhao, L., Zhang, H., Zhao, B. & Lyu, H. 2022 Activation of peroxydisulfate by ball-milled α-FeOOH/biochar composite for phenol removal: Component contribution and internal mechanisms. *Environmental Pollution* **293**, 118596.

Zhong, M., Wang, T., Zhao, W., Huang, J., Wang, B., Blaney, L., Bu, Q. & Yu, G. 2022 Emerging organic contaminants in Chinese surface water: Identification of priority pollutants. *Engineering* **11**, 111–125.

Zhou, Y., Jiang, J., Gao, Y., Ma, J., Pang, S., Li, J., Lu, X. & Yuan, L. 2015 Activation of peroxymonosulfate by benzoquinone: A novel nonradical oxidation process. *Environmental Science & Technology* **49** (21), 12941–12950.

Zhou, J., Yang, X., Wei, Q., Lan, Y. & Guo, J. 2023 Co_3O_4 anchored on biochar derived from chitosan (Co_3O_4@BCC) as a catalyst to efficiently activate peroxymonosulfate (PMS) for degradation of phenacetin. *Journal of Environmental Management* **327**, 116895.

Zhu, Y., Zhu, R., Xi, Y., Zhu, J., Zhu, G. & He, H. 2019 Strategies for enhancing the heterogeneous Fenton catalytic reactivity: A review. *Applied Catalysis B: Environmental* **255**, 117739.

Zhu, F., Wu, Y., Liang, Y., Li, H. & Liang, W. 2020a Degradation mechanism of norfloxacin in water using persulfate activated by BC@nZVI/Ni. *Chemical Engineering Journal* **389**, 124276.

Zhu, K., Bin, Q., Shen, Y., Huang, J., He, D. & Chen, W. 2020b In-situ formed N-doped bamboo-like carbon nanotubes encapsulated with Fe nanoparticles supported by biochar as highly efficient catalyst for activation of persulfate (PS) toward degradation of organic pollutants. *Chemical Engineering Journal* **402**, 126090.

Zhu, J., Song, Y., Wang, L., Zhang, Z., Gao, J., Tsang, D. C. W., Ok, Y. S. & Hou, D. 2022 Green remediation of benzene contaminated groundwater using persulfate activated by biochar composite loaded with iron sulfide minerals. *Chemical Engineering Journal* **429**, 132292.

Zhuang, Y., Lin, Q., Zhang, L., Lianshun, L. & Yuyuan, Y. 2016 Mesoporous carbon-supported cobalt catalyst for selective oxidation of toluene and degradation of water contaminants. *Particuology* **24**, 216–222.

First received 26 February 2024; accepted in revised form 15 July 2024. Available online 25 July 2024